Periodic orbits above the ecliptic in the solar sail restricted 3-body problem

Thomas J. Waters *and Colin R. McInnes †

Department of Mechanical Engineering, University of Strathclyde, Glasgow, G1 1XJ, Scotland, UK.

We consider periodic orbits in the circular restricted 3-body problem, where the third (small) body is a solar sail. In particular, we consider orbits about equilibrium points in the Earth-Sun rotating frame which are high above the ecliptic plane, in contrast to the classical 'halo' orbits about the collinear equilibria. It is found that due to coupling in the equations of motion, periodic orbits about equilibria are naturally present at linear order. Using the method of Lindstedt-Poincaré, we construct nth order approximations to periodic solutions of the nonlinear equations of motion. It is found that there is much freedom in specifying the position and period/amplitude of the orbit of the sail, high above the ecliptic and looking down on the Earth. A particular use of such solutions is presented, namely the year-round constant imaging of, and communication with, the poles. We find that these orbits present a significant improvement on the position of the sail when viewed from the Earth, compared to a sail placed at equilibrium.

1. Introduction

While the concept of the solar sail has been with us for some time, it is only with recent advances in materials and structures that their use is being seriously considered. A solar sail consists essentially of a large mirror, which uses the momentum change due to photons reflecting off the sail for its impulse. A natural setting to consider the orbital dynamics of a solar sail is the circular restricted 3-body problem (CRTBP), with the Earth and Sun as the two primaries. The classical CRTBP admits five well-known equilibrium points, the Lagrange points, all of which are in the plane of the primaries mutual orbit. However, when we consider the small body to be a solar sail, we find that due to the non-central nature of the force on the solar sail there are instead continuous surfaces of equilibrium points in the three-dimensional space.

There has been some work already carried out regarding solar sails in the 3-body problem. McInnes et al.[1] first described the surfaces of equilibrium points, and some possible uses of same. In Baoyin and

*Research Fellow, thomas.waters@strath.ac.uk

†Professor, colin.mcinnes@strath.ac.uk, member AIAA

McInnes[2] and McInnes,[3] the authors describe periodic orbits about equilibrium points in the solar sail three body problem, however they consider only equilibrium points on the axis joining the primary masses, corresponding to artificial Lagrange points. Such orbits are analogous to the classical 'halo' orbits, which are well documented, for example Farquhar,[4] Farquhar and Kamel,[5] Breakwell and Brown,[6] Richardson,[7] Howell[8] and Thurman and Worfolk.[9] Small amplitude orbits about equilibria are further considered in Baoyin and McInnes,[10] while the generalization to the elliptical restricted 3-body problem is considered in Baoyin and McInnes.[11] The orbit of a solar sail about an asteroid in Hill's problem was considered in Morrow, Scheeres and Lubin,[12] and the equilibria available to a non-perfect solar sail were described in McInnes.[13] Detailed applications for artificial equilibria on the night-side of the Earth can be found in Forward,[14] and there have been various studies of applications of day-side equilibria for Earth observation, see for example Crison.[15]

The existence of equilibrium points out of the ecliptic plane has lead to the possibility of new and interesting orbits, which conventional spacecraft are not capable of. Of particular interest with regards this work is the possibility of putting a solar sail in an orbit from which it would be able to constantly view the polar regions and high latitudes. In a frame rotating with the Earth, the orientation of the Earth's axis of rotation will vary over the course of a year, and to provide a continuous view of the poles the solar sail's orbit would need to counter this effect. We show how this may be accomplished to a large degree by constructing large amplitude periodic orbits about the out-of-plane equilibria.

In the next section we describe the equations of motion of the solar sail in the restricted 3-body problem. In Section 3 we examine the solutions to the linearised equations of motion and discuss their stability. We find that periodic orbits exist naturally at linear order, and in Section 4 we use these linear solutions to find higher order approximations to periodic solutions to the non-linear system using the method of Lindstedt-Poincaré. In Section 5 we briefly describe a differential corrector algorithm which fine-tunes the initial data which these approximations provide to give periodic solutions to the full non-linear system. In Section 6 we use these periodic orbits to consider a specific use of the solar sail: the year-round constant observation of the poles. We show how, by timing the orbit of the sail appropriately, we may greatly narrow the annual variation in the elevation angle of the sail above the local horizon when viewed from the poles.

As the analysis we will use is closely analogous to that of the 'halo' orbits in the classical CRTBP, we will be careful to point out any significant differences between the two settings.

2. Equations of motion

We will follow the conventions set out in McInnes.[16] As there are no natural equilibria in the inertial frame we will consider a rotating frame of reference in which the primary masses are fixed. The x-axis points between the primary masses, the z-axis is the axis of rotation, and the y-axis completes the triad. The

angular velocity of the frame is therefore $\boldsymbol{\omega} = \widehat{\boldsymbol{z}}$ (where $\widehat{\boldsymbol{v}}$ denotes a unit vector pointing in the direction of $\boldsymbol{v}$). We chose our units to set the gravitational constant, the sum of the primary masses, the distance between the primaries, and the magnitude of the angular velocity of the rotating frame to be unity. We shall denote by $\mu = 3 \times 10^{-6}$ the dimensionless mass of the smaller body m_2, the Earth, and therefore the mass of the larger body m_1, the Sun, is given by $1 - \mu$ (see Figure 1).

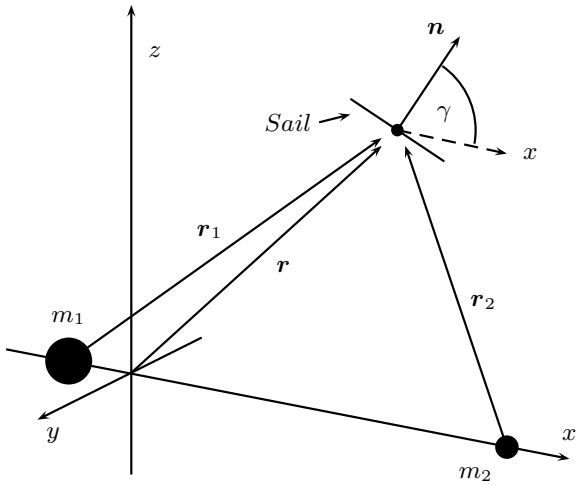

Figure 1. The rotating coordinate frame and the sail position therein.

We will take our origin of coordinates as the centre of mass of the two primaries, and we denote with $\boldsymbol{r}_1$ and $\boldsymbol{r}_2$ the position vectors of the sail with respect to m_1 and m_2 respectively, with

$$\boldsymbol{r}_1 = (x + \mu, y, z)^T, \qquad \boldsymbol{r}_2 = (x - (1 - \mu), y, z)^T.$$

The position vector of the sail is given by $\boldsymbol{r} = (x, y, z)^T$, and in the rotating coordinate frame the vector equations of motion are given by (dots denoting differentiation with respect to time, t, relative to the rotating frame)

$$\ddot{\boldsymbol{r}} + 2\,\boldsymbol{\omega} \times \dot{\boldsymbol{r}} = \nabla V + \boldsymbol{a} \equiv \boldsymbol{F}, \tag{1}$$

where V is the augmented potential given by

$$V = \left(\frac{1 - \mu}{r_1} + \frac{\mu}{r_2} \right) + \tfrac{1}{2} |\boldsymbol{\omega} \times \boldsymbol{r}|^2,$$

with $r_1 = |\boldsymbol{r}_1|$ etc. Here $\boldsymbol{a}$ is the acceleration of the sail due to the radiation pressure from the Sun, and is given by[16]

$$\boldsymbol{a} = \beta \frac{1 - \mu}{r_1^2}\, (\widehat{\boldsymbol{r}}_1 . \boldsymbol{n})^2\, \boldsymbol{n}, \tag{2}$$

where $\boldsymbol{n}$ is the unit normal to the sail. β is the sail lightness number, and is the ratio of the solar radiation pressure acceleration to the solar gravitational acceleration.

The sail normal is most generally given in terms of the clock and cone angles (see [16]), however in this article we will consider the sail normal to point in the x-z plane, as we are interested in equilibria in the x-z plane. With γ denoting the angle the sail normal makes with the x-axis, we may write

$$\boldsymbol{n} = \cos(\gamma)\widehat{\boldsymbol{x}} + \sin(\gamma)\widehat{\boldsymbol{z}}.$$

Thus there are two-parameter families of equilibria (one on the L_1 side and one on the L_2 side), defined by fixing β and γ and solving $\boldsymbol{F} = 0$ for the coordinates of equilibrium (the y-coordinate will be zero). Alternatively, we may choose the equilibrium coordinates required and then solve for the appropriate values of β and γ.

Letting $\boldsymbol{r}_e = (x_e, 0, z_e)^T$ denote an equilibrium point in the x-z plane, we find the β and γ values necessary to put the sail at this equilibrium point are

$$\tan(\gamma) = z\mathcal{V}\left(\frac{(1-\mu)(x+\mu)}{r_1^3} + \frac{\mu(x-1+\mu)}{r_2^3} - x\right)^{-1}\Bigg|_e, \tag{3}$$

$$\beta = z\, r_1^4 \mathcal{V}\Big((1-\mu)\sin(\gamma)\big[(x+\mu)\cos(\gamma) + z\sin(\gamma)\big]\Big)^{-1}\Big|_e, \tag{4}$$

where $\mathcal{V} = \left[\frac{1-\mu}{r_1^3} + \frac{\mu}{r_2^3}\right]$. Using these expressions we may calculate surfaces of equilibrium points in the x_e-z_e parameter space, see Figure 2. We note that in this work we are considering a perfectly reflecting solar sail, and the equilibrium curves for a non-perfect sail are slightly different; see McInnes.[13]

While a β value of about $0.3 - 0.4$ is considered within the realm of possibility, to put the analysis in this paper well within the near-term we will consider very modest β values of about 0.05.

3. Linearised system

We linearise about the equilibrium point by making the transformation $\boldsymbol{r} \to \boldsymbol{r}_e + \delta\boldsymbol{r}$, Taylor expanding $\boldsymbol{F}$ about $\boldsymbol{r}_e$, and neglecting the terms quadratic in $\delta\boldsymbol{r}$. We assume the orientation of the sail will remain fixed under perturbation of the sail position, in which case γ and β are constants, and we may use the expressions given in (4). Letting $\delta\boldsymbol{r} = (\delta x, \delta y, \delta z)^T$ and $\boldsymbol{X} = (\delta\boldsymbol{r}, \delta\dot{\boldsymbol{r}})^T$, our linear system is $\dot{\boldsymbol{X}} = A\boldsymbol{X}$ with

$$A = \left(\begin{array}{c|c} 0 & I \\ \hline M & \Theta \end{array}\right), \qquad M = \begin{pmatrix} a & 0 & b \\ 0 & c & 0 \\ d & 0 & e \end{pmatrix}, \qquad \Theta = \begin{pmatrix} 0 & 2 & 0 \\ -2 & 0 & 0 \\ 0 & 0 & 0 \end{pmatrix}, \tag{5}$$

where

$$a = (\partial_x F^x)|_e, \quad b = (\partial_z F^x)|_e, \quad c = (\partial_y F^y)|_e, \quad d = (\partial_x F^z)|_e, \quad e = (\partial_z F^z)|_e,$$

and $b \neq d$. Here F^a denotes the a-th component of $\boldsymbol{F}$, and M is sparse due to $y_e = 0$.

The key difference between this analysis and the classical orbits about the collinear Lagrange points is the term $d \neq 0$, which appears precisely because we are linearising about an equilibrium point with $z_e \neq 0$. This

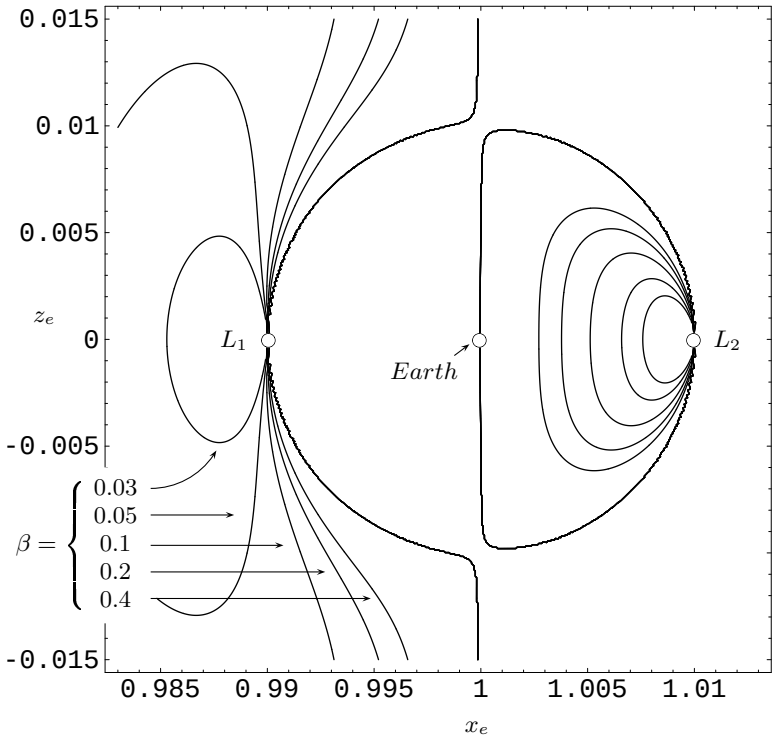

Figure 2. Surfaces of equilibrium points in the x_e-z_e parameter space. Each curve is specified by a constant value of β, and the position of the equilibrium point along the curve is given by γ.

means we cannot decouple the z-equation. While this initially seems to make the problem more complicated, we can use this to our advantage, as will be made clear.

The characteristic equation of the linear coefficient matrix A, the Jacobian, is bi-cubic; this simplifies the analysis of the eigenvalues. If we denote the characteristic equation of the Jacobian as $P(\lambda) = \lambda^6 + a_1\lambda^4 + a_2\lambda^2 + a_3 = 0$, then there is a corresponding cubic equation in $\eta = \lambda^2$, $\bar{P}(\eta) = \eta^3 + a_1\eta^2 + a_2\eta + a_3 = 0$. The roots of this equation are always real, and we find one is always positive, one always negative, and the third changes sign in the regions depicted in Figure 3. We label region I and II as the regions where the third root is negative (analogous to the collinear Lagrange points) and positive respectively. Therefore the spectrum of the Jacobian in region I is

$$I : \left\{\lambda_1 i, -\lambda_1 i, \lambda_2 i, -\lambda_2 i, \lambda_r, -\lambda_r\right\},$$

and we denote the eigenvectors associated with $\lambda_a i$ $(a = 1, 2)$ as $\boldsymbol{u}_a + \boldsymbol{w}_a i$, and the eigenvectors associated with $\lambda_r, -\lambda_r$ as $\boldsymbol{v}_1, \boldsymbol{v}_2$, with

$$\boldsymbol{u}_a = \left(-(e+\lambda_a^2), 0, d, 0, \tfrac{2\lambda_a^2(e+\lambda_a^2)}{(c+\lambda_a^2)}, 0\right)^T, \qquad \boldsymbol{w}_a = \left(0, \tfrac{-2\lambda_a(e+\lambda_a^2)}{(c+\lambda_a^2)}, 0, -\lambda_a(e+\lambda_a^2), 0, \lambda_a d\right)^T.$$

The general solution in region I is therefore[17]

$$\begin{aligned}\boldsymbol{X}(t) =& \cos(\lambda_1 t)\big[A\boldsymbol{u}_1 + B\boldsymbol{w}_1\big] + \sin(\lambda_1 t)\big[B\boldsymbol{u}_1 - A\boldsymbol{w}_1\big] \\ &+ \cos(\lambda_2 t)\big[C\boldsymbol{u}_2 + D\boldsymbol{w}_2\big] + \sin(\lambda_2 t)\big[D\boldsymbol{u}_2 - C\boldsymbol{w}_2\big] \\ &+ Ee^{\lambda_r t}\boldsymbol{v}_1 + Fe^{-\lambda_r t}\boldsymbol{v}_2. \end{aligned} \tag{6}$$

There are no complex eigenvalues of the Jacobian since there are no imaginary roots to $\bar{P}(\eta) = 0$; consequently the dynamical nature of equilibria is centres crossed with saddles.

We may choose our initial data to set $E = F = 0$ and switch off the real modes, in which case the solutions describe 'roses' in the x-y and y-z planes, due to the mixing of frequencies in the solution (6). However, we may go a step further and set $C = D = 0$ (or $A = B = 0$), and thus our solution may be written

$$\delta x = kA_z \cos(\lambda_a t + \phi), \qquad \delta y = mA_z \sin(\lambda_a t + \phi), \qquad \delta z = A_z \cos(\lambda_a t + \phi), \tag{7}$$

with $k = u_a^1/u_a^3$ and $m = -w_a^2/u_a^3$. Here $\lambda_a = \lambda_1$ or λ_2 depending on which pair we choose to set equal to zero, A, B or C, D. Thus in this problem there are periodic solutions at linear order (by restricting initial data), in contrast to orbits about the collinear equilibrium points where we must add artificial terms to force the in-plane and out-of-plane frequencies of quasi-periodic Lissajous orbits to be equal. This means we do not need to use nonlinear terms to force periodic orbits, as they happen naturally. This is due to the coupling in the $\delta x, \delta y, \delta z$ equations, which in turn is due to our choice of $z_e \neq 0$.

The qualitative nature of equilibria in region II is the same, only here the spectrum is

$$II : \big\{\lambda_1 i, -\lambda_2 i, \lambda_{r_1}, -\lambda_{r_1}, \lambda_{r_2}, -\lambda_{r_2}\big\}.$$

There is only one pair of imaginary conjugate eigenvalues, and two pairs of real eigenvalues, however by choosing initial data we will again have periodic solutions as in (7), the only difference being we are not free to choose the frequency.

4. Nonlinear approximations

We use the method of Lindstedt-Poincaré (or strained coordinates) to find periodic approximations to the nonlinear solution. The idea behind the method is to assume that the nonlinear solution is periodic with a frequency which is a perturbation of the linear solution's. This method has been used quite extensively throughout the literature.[2,7,9]

First we continue the Taylor expansion of $\boldsymbol{F}$ about the equilibrium point to nth order, giving the system

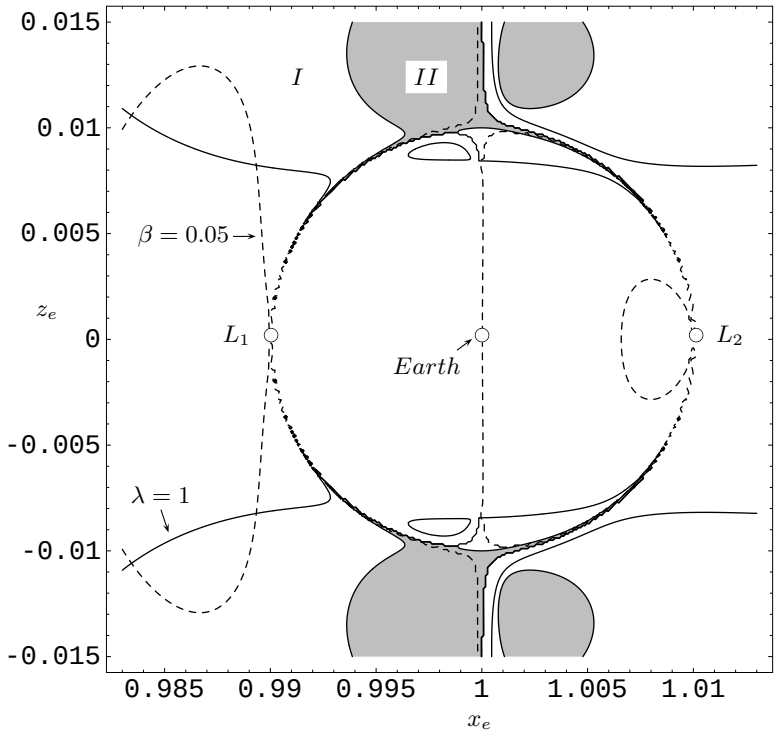

Figure 3. The regions in parameter space in which the third root (to the cubic equation corresponding to the characteristic equation of A) is negative (I) or positive (II). The curve on which the lesser of the linear order frequencies is unity is shown, and the $\beta = 0.05$ curve is shown dashed for reference.

of equations

$$\begin{pmatrix} \ddot{x} - 2\dot{y} \\ \ddot{y} + 2\dot{x} \\ \ddot{z} \end{pmatrix} = \delta r^a (\partial_a \boldsymbol{F})|_e + \tfrac{1}{2}\,\delta r^a\,\delta r^b (\partial_a \partial_b \boldsymbol{F})|_e + \tfrac{1}{6}\,\delta r^a\,\delta r^b\,\delta r^c (\partial_a \partial_b \partial_c \boldsymbol{F})|_e + O(\delta \boldsymbol{r}^4),$$

with summation over repeated indices implied. $(\partial_a \boldsymbol{F})|_e$ is the linearised matrix M given before.

Next we introduce the small parameter ε and expand each of the variables up to third order in ε, as in $x \to \varepsilon x_1 + \varepsilon^2 x_2 + \varepsilon^3 x_3 + O(\varepsilon^4)$ etc. Then we introduce a new time coordinate $\tau = \omega t$, with $\omega = 1 + \varepsilon\omega_1 + \varepsilon^2\omega_2 + O(\varepsilon^3)$, such that $x_1 = x_1(\tau)$ and so on. We let a prime denote differentiation with respect to τ. Finally we group together powers of ε to give a system of equations at each order of ε.

At first order the system of equations is identical to the linear system (5),

$$\begin{aligned} x_1'' - 2y_1' - ax_1 - bz_1 &= 0 \\ y_1'' + 2x_1' - cy_1 &= 0 \\ z_1'' - dx_1 - ez_1 &= 0. \end{aligned}$$

Again we point out the crucial role played by the term $d \neq 0$, resulting in the full coupling of the equations.

For periodic solutions, we let our first order solution be (see (7))

$$x_1 = kA_z\cos(T), \qquad y_1 = mA_z\sin(T), \qquad z_1 = A_z\cos(T),$$

with $T = \lambda\tau + \phi$ and k, m as defined previously.

At second order we find

$$\begin{aligned} x_2'' - 2y_2' - ax_2 - bz_2 &= \alpha_{20} + \omega_1\alpha_{21}\cos(T) + \alpha_{22}\cos(2T), \\ y_2'' + 2x_2' - cy_2 &= \omega_1\beta_{21}\sin(T) + \beta_{22}\sin(2T), \\ z_2'' - dx_2 - ez_2 &= \gamma_{20} + \omega_1\gamma_{21}\cos(T) + \gamma_{22}\cos(2T). \end{aligned} \tag{8}$$

Here $\alpha_{21}, \beta_{21}, \gamma_{21}$ are functions of the coefficients of the Taylor expansion of $\boldsymbol{F}$, and thus are not free variables; we must set $\omega_1 = 0$ to prevent secular terms in the solution. Therefore our second order solution is

$$x_2 = p_{20} + p_{22}\cos(2T), \qquad y_2 = q_{22}\sin(2T), \qquad z_2 = s_{20} + s_{22}\cos(2T),$$

where the coefficients p_{20} etc. are given later in (12).

At third order we have

$$\begin{aligned} x_3'' - 2y_3' - ax_3 - bz_3 &= \alpha_{31}\cos(T) + \alpha_{33}\cos(3T), \\ y_3'' + 2x_3' - cy_3 &= \beta_{31}\sin(T) + \beta_{33}\sin(3T), \\ z_3'' - dx_3 - ez_3 &= \gamma_{31}\cos(T) + \gamma_{33}\cos(3T). \end{aligned} \tag{9}$$

Here α_{31}, β_{31} and γ_{31} are functions of our two free variables, A_z and ω_2; thus we do not need to 'switch off' resonant terms, for the following reason: while

$$\{x = B_1\cos(T),\ y = B_2\sin(T),\ z = B_3\cos(T)\}$$

is a solution of the left hand side of this system, we see that, since the equations are fully coupled, only the three of these together solves the left hand side exactly. Setting one or two of the solutions to zero no longer solves the left hand side exactly, and may solve the right hand side if the coefficients α_{31}, β_{31} and γ_{31} satisfy certain equations. However, α_{31}, β_{31} and γ_{31} are functions of the free variables and thus we may choose A_z, ω_2 to make the coefficients satisfy these equations.

Studying the left hand side of the system we see there are two choices,

$$\begin{aligned} &(i) \quad \{x = B_1\cos(T),\ y = 0,\ z = 0\}, \\ &(ii) \quad \{x = 0,\ y = B_2\sin(T),\ z = B_3\cos(T)\}. \end{aligned}$$

The first option means A_z and ω_2 must satisfy two equations, whereas the second option requires only the one. Therefore there is more freedom left over with the second choice, and we find A_z and ω_2 must satisfy the constraint

$$\frac{2\lambda\beta_{31}}{(c+\lambda^2)} + \frac{b\gamma_{31}}{(e+\lambda^2)} - \alpha_{31} = 0,$$

which reduces to

$$\omega_2 = \ell_2 A_x^2.$$

Then our third order solutions are

$$x_3 = p_{33}\cos(3T), \qquad y_3 = q_{31}\sin(T) + q_{33}\sin(3T), \qquad z_3 = s_{31}\cos(T) + s_{33}\cos(3T),$$

where the coefficients p_{33} etc. are given in (10), (12), and q_{31}, s_{31} correspond to B_2, B_3 above.

Third order approximations are sufficiently close to the true periodic solutions to the non-linear system (1) to make a differential corrector (see next section) converge, only when the equilibrium point is low on the ecliptic plane (as in the classical halo orbits) or when the amplitude is small ($A_z \sim 10^{-4}$). However, for equilibrium points high above the ecliptic plane and with large amplitudes ($A_z \sim 10^{-2}$), it is necessary to find higher order approximations. Thus we may generalise the above analysis in the following way:

At each order of approximation n, we find $\omega_{n-1} = 0$ if n is even, and $\omega_{n-1} \neq 0$ if n is odd; this is due to the fact that (leaving out the coefficients for brevity)

$$\cos^n(\theta) \sim \begin{cases} 1 + \cos(2\theta) + \ldots + \cos(n\theta) & n \text{ even}, \\ \cos(\theta) + \ldots + \cos(n\theta) & n \text{ odd}, \end{cases}$$

with a similar expression for $\sin^n(\theta)$.

The inhomogeneous part to the equations at order n therefore has the following form: when n is odd, as in (9)

$$\begin{aligned} \alpha_{n1}\cos(T) + \ldots + \alpha_{nn}\cos(nT), \\ \beta_{n1}\sin(T) + \ldots + \beta_{nn}\sin(nT), \\ \gamma_{n1}\cos(T) + \ldots + \gamma_{nn}\cos(nT), \end{aligned}$$

and when n is even, as in (8)

$$\begin{aligned} \alpha_{n0} + \alpha_{n2}\cos(2T) + \ldots + \alpha_{nn}\cos(nT), \\ \beta_{n2}\sin(2T) + \ldots + \beta_{nn}\sin(nT), \\ \gamma_{n0} + \gamma_{n2}\cos(2T) + \ldots + \gamma_{nn}\cos(nT). \end{aligned}$$

When n is odd, the solutions at nth order have the form

$$\begin{aligned} x_n = {} & p_{n3}\cos(3T) + \ldots + p_{nn}\cos(nT), \\ y_n = {} & q_{n1}\sin(T) + q_{n3}\sin(3T) + \ldots + q_{nn}\sin(nT), \\ z_n = {} & s_{n1}\cos(T) + s_{n3}\cos(3T) + \ldots + s_{nn}\cos(nT), \end{aligned}$$

with

$$q_{n1} = \frac{-\beta_{n1}}{(c+\lambda^2)}, \qquad s_{n1} = \frac{-\gamma_{n1}}{(e+\lambda^2)}, \tag{10}$$

and ω_{n-1} solves

$$\frac{2\lambda\beta_{n1}}{(c+\lambda^2)} + \frac{b\gamma_{n1}}{(e+\lambda^2)} - \alpha_{n1} = 0, \tag{11}$$

which reduces to $\omega_{n-1} = \ell_{n-1}A_x^{n-1}$.

When n is even, the nth order solutions have the form

$$\begin{aligned} x_n =& p_{n0} + p_{n2}\cos(2T) + \ldots + p_{nn}\cos(nT), \\ y_n =& \qquad q_{n2}\sin(2T) + \ldots + q_{nn}\sin(nT), \\ z_n =& s_{n0} + s_{n2}\cos(2T) + \ldots + s_{nn}\cos(nT). \end{aligned}$$

At each order, odd or even, the coefficients (with $j \neq 1$) are found from

$$q_{nj} = \frac{-2j\lambda p_{nj} - \beta_{nj}}{(c+j^2\lambda^2)}, \qquad s_{nj} = \frac{-dp_{nj} - \gamma_{nj}}{(e+j^2\lambda^2)}, \qquad -(a+j^2\lambda^2)p_{nj} - 2j\lambda q_{nj} - bs_{nj} - \alpha_{nj} = 0. \tag{12}$$

5. Differential Corrector

The series given above are only periodic approximations to solutions to the full non-linear system (1). If we take these approximations and set $t = \tau = 0$ and use this as initial data to integrate (1), we find the trajectories quickly diverge from periodicity, especially when we choose an equilibrium point high above the ecliptic plane. Instead, we use these approximations as a first seed in a differential corrector to fine tune the initial data to close the trajectory. Differential correctors are described in much detail in the literature regarding halo orbits,[6,7,9] and as the present situation is closely analogous we merely sketch the procedure here.

As our periodic approximations are trigonometric Cosine series in x and z, and Sine series in y, our initial data has the form

$$\boldsymbol{X}(0) = (x_0, 0, z_0, 0, \dot{y}_0, 0)^T,$$

where $\boldsymbol{X}(t)$ from now on represents the trajectory's position in phase-space, and $\dot{\boldsymbol{X}} = \boldsymbol{f}(\boldsymbol{X})$ as in (1). On returning to the $y = 0$ plane at time $t = T_{1/2}$, we have

$$\boldsymbol{X}(T_{1/2}) = (\tilde{x}, 0, \tilde{z}, \dot{\tilde{x}}, \dot{\tilde{y}}, \dot{\tilde{z}}),$$

and our orbit is periodic when $\dot{\tilde{x}} = \dot{\tilde{z}} = 0$.

We may vary the initial conditions to force periodic orbits. Letting

$$x_0 \to x_0 + \Delta x, \quad z_0 \to z_0 + \Delta z, \quad \dot{y}_0 \to \dot{y}_0 + \Delta\dot{y}_0, \quad T_{1/2} \to T_{1/2} + \Delta T_{1/2},$$

and by linearising the periodicity conditions we have the matrix equation

$$\begin{pmatrix} \dot{x} \\ \dot{z} \\ y \end{pmatrix} + \begin{pmatrix} \frac{\partial \dot{x}}{\partial x_0} & \frac{\partial \dot{x}}{\partial z_0} & \frac{\partial \dot{x}}{\partial \dot{y}_0} & \frac{\partial \dot{x}}{\partial T_{1/2}} \\ \frac{\partial \dot{z}}{\partial x_0} & \frac{\partial \dot{z}}{\partial z_0} & \frac{\partial \dot{z}}{\partial \dot{y}_0} & \frac{\partial \dot{z}}{\partial T_{1/2}} \\ \frac{\partial y}{\partial x_0} & \frac{\partial y}{\partial z_0} & \frac{\partial y}{\partial \dot{y}_0} & \frac{\partial y}{\partial T_{1/2}} \end{pmatrix} \begin{pmatrix} \Delta x \\ \Delta z \\ \Delta \dot{y} \\ \Delta T_{1/2} \end{pmatrix} = 0,$$

where the matrix of partial derivatives contains elements of the state transition matrix.

There are three equations here and four variables. Usually, Δz is set to zero and this is used to draw the initial data close to a periodic orbit while keeping the amplitude large. However, there is also the option in letting $\Delta x, \Delta z$ and $\Delta \dot{y}$ vary, and using the remaining freedom to choose $\Delta T_{1/2}$. This is useful when we wish to fine tune the period of the orbit, for example in the next section where we may let $\Delta T_{1/2} = T_{1/2} - \pi$ to make the period close to one year (2π in non-dimensional units). For this to converge we must have an orbit already close to periodic with half-period quite close to the required value.

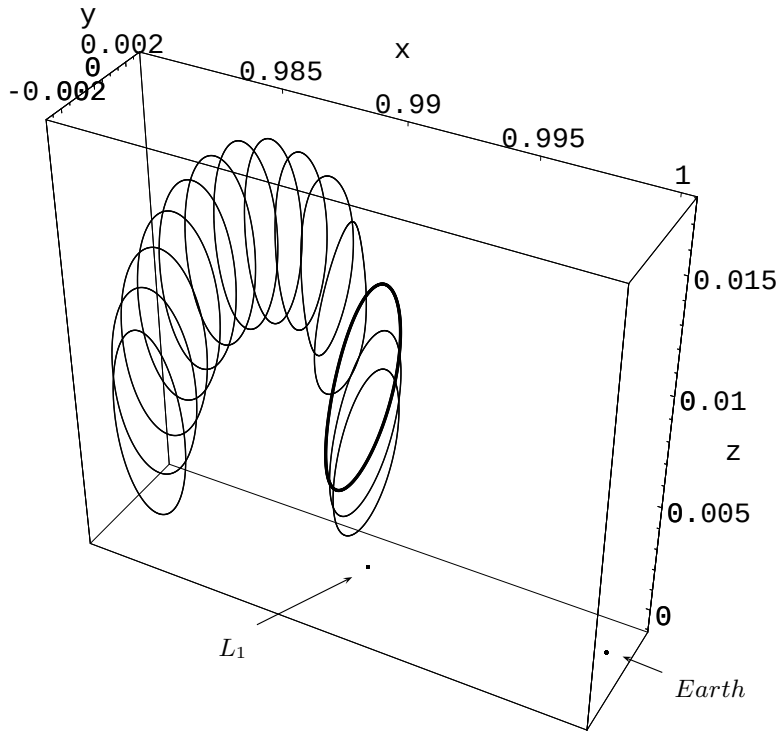

Figure 4. A family of orbits with $\beta = 0.05174$, as in the reference orbit described in Section 6. Each orbit has amplitude $A_z = 0.0038$ and is about a different equilibrium point along the β level curve shown in Figure 2, each equilibrium point being defined by a different γ value. The one-year orbit of the Section 6 is heavily drawn, and has $\gamma = 0.8092$. For reference the Earth (to scale) and L_1 are shown.

To finish, we find a 3-parameter family of periodic orbits, each defined by the set $\{\beta, \gamma, A_z\}$. Assuming a particular solar sail will have a fixed β parameter, various families of periodic orbits accessible to the sail are defined by $\{\gamma, A_z\}$. We present the variations in these parameters in Figures 4 and 5. In Figure 4 we fix

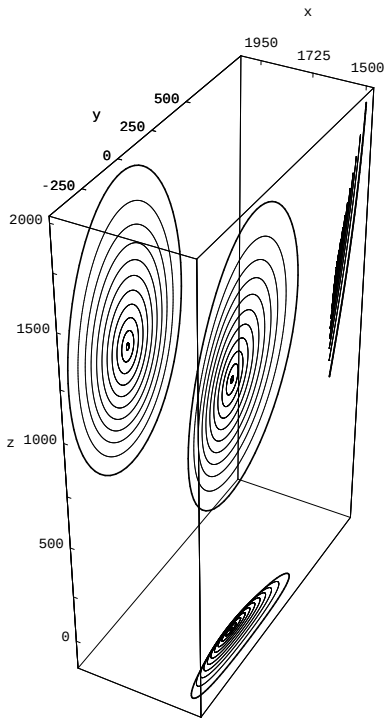

Figure 5. Some periodic orbits about the equilibrium point $x_e = 0.9895$, $z_e = 0.0078$,; we also show the projection of these orbits in the x-y, y-z and x-z planes. In this plot we give the units in $10^3 km$, with the x-axis showing distance from the Earth. The largest orbit has $A_z = 0.0038$ and is the reference orbit used in Section 6.

the amplitude and let the γ value vary, forming a 'tube' of periodic orbits, whereas in Figure 5 we fix γ and let the amplitude vary, forming a paraboloid-type surface of periodic orbits.

6. One year orbits

A closed orbit with period one year will counter the seasonal effect of the variation of the Earth's axis of rotation in the rotating frame, if we time the orbit appropriately, as in Figure 6. For constant observation of the North pole (the set-up is, of course, symmetric in the ecliptic plane), we let the sail be at the highest point of its orbit during the Wintertime, $t = 0$, and at the lowest point of its orbit during the Summertime, $t = \pi$. Then the variation in elevation of the sail above the local horizon when viewed from the north pole will be greatly narrowed over the course of a year.

The equilibrium point about which the sail is to orbit needs to be chosen carefully. The Lindstedt-Poincaré method gives us an approximation to the nonlinear frequency, $\omega\lambda$, where λ is the frequency at linear order and $\omega = 1 + \omega_2\varepsilon^2 + \omega_4\varepsilon^4 + \omega_6\varepsilon^6 + O(\varepsilon^8)$. To match the orbital frequency of the Earth, that is for $\omega\lambda = 1$, we should choose an equilibrium point close to the region where $\lambda = 1$ as shown in Figure 3. Also

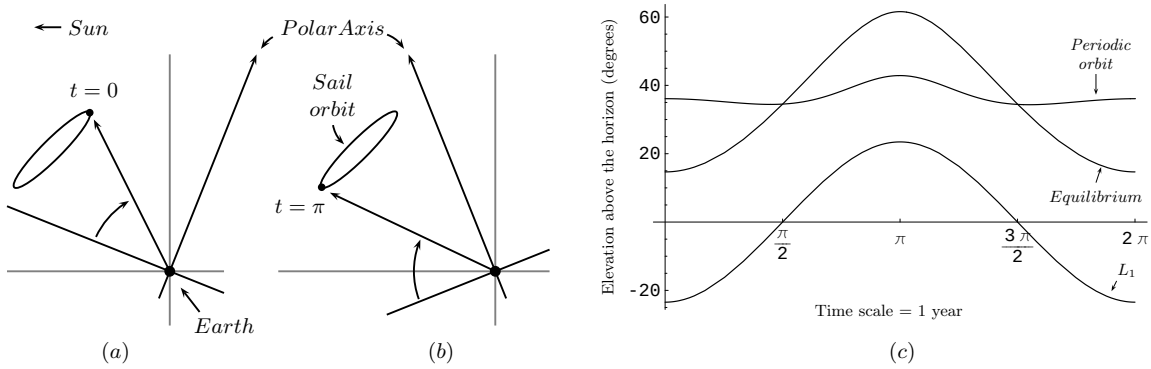

Figure 6. One year orbits which counter the seasonal variation in the Earth's axis of rotation. Schematically the sail's position (in the rotating frame) is shown in (a) Wintertime and (b) Summertime in the northern hemisphere. The elevation of the sail above the horizon over one year (or 2π in non-dimensional units) is shown in (c), with the elevation of a sail fixed at the equilibrium point and at L_1 also shown for reference.

we must choose an equilibrium point which requires a reasonable β. For illustrative purposes, we choose a reference equilibrium point

$$x_e = 0.9895, \quad z_e = 0.0078,$$

as this equilibrium point requires $\beta = 0.05174$ (which correspods to a sail loading of 30 g/m^2 or a characteristic acceleration of 0.3 mm/s^2) and has a linear frequency $\lambda \sim 1.04$. We note that this orbit will be on the L_1 side of the Earth; as we can see from Figure 3, a reasonable β value will not be close to the $\lambda = 1$ region on the L_2 side of the Earth.

Using the methods presented in Section 4, we may find approximations to periodic orbits about this equilibrium point, and for completeness we present the coefficients of the 7^{th} order approximation in Table 1 as a function of the amplitude A_z.

Using these approximations, a differential corrector will converge for values of $A_z < 0.004$. We run the differential corrector (keeping the z-coordinate fixed) a number of times until the orbit is almost closed; then by allowing each coordinate to vary and forcing $T_{1/2} = \pi$, we may fine-tune the initial data to get a periodic orbit of period exactly one year. The result is in Figures 4 and 5.

The effect of such an orbit on the position of the sail when viewed from the North pole is shown in Figure 6 (c). We see the angle subtended by the sail has narrowed to about 11°, a significant improvement over the 46° subtended by a sail at the equilibrium point.

We note a useful combination is to place one sail at the equilibrium point and allow a second sail to orbit it in a large periodic orbit, corresponding to formation-flying when viewed from an inertial frame. This would provide contrasting viewpoints for stereo Earth observation.

For completeness, we show in Figure 7 some possible trajectories to insert a solar sail from the vicinity of the Earth onto the large amplitude reference periodic orbit. To calculate these trajectories we use Floquet

theory to derive the variational equations and calculate the monodromy matrix. As this has been discussed in great detail elsewhere and is not the main thrust of this paper, we include only a brief description and refer the reader to [9,17,18].

Let $\boldsymbol{X} = (\boldsymbol{r}, \dot{\boldsymbol{r}})$ and let the nonlinear system (1) be written $\dot{\boldsymbol{X}} = \boldsymbol{f}(\boldsymbol{X})$. Let $\boldsymbol{\Gamma}(t)$ denote a periodic solution to this system, with period T. By letting $\boldsymbol{X} = \boldsymbol{\Gamma} + \boldsymbol{Y}$, we may linearise the nonlinear system about this periodic solution, resulting in the variational equations

$$\dot{\boldsymbol{Y}} = \frac{\partial \boldsymbol{f}}{\partial \boldsymbol{X}}\Big|_{\boldsymbol{X}=\boldsymbol{\Gamma}} \boldsymbol{Y} \equiv A(t)\ \boldsymbol{Y}, \tag{13}$$

where $A(t+T) = A(t)$. This is a non-autonomous linear system with periodic coefficients. A well known result of Floquet theory is that for every fundamental solution matrix of a system such as (13), there is a non-singular constant matrix B such that

$$Y(T) = Y(0)\, B. \tag{14}$$

Therefore the eigenvalues of B tell us about the linear stability of the periodic orbit. Recasting the variational equations in terms of the state transition matrix (or principal fundamental matrix) $\Phi = \partial \boldsymbol{X}/\partial \boldsymbol{X}(0)$ already referred to in Section 5, we have

$$\dot{\Phi} = A(t)\Phi, \qquad \Phi(0) = I,$$

and thus we asscociate the matrix B given in (14) with $\Phi(T)$, the monodromy matrix.

As the divergence of our original system vanishes, that is the trace of the Jacobian $\sum \partial f^i/\partial X_i = 0$ (see (5)), Louiville's theorem (constancy of volume in phase space) applies. Thus[18] the eigenvalues of the monodromy matrix occur in reciprocal pairs, two of them are unity, and stability of the periodic orbit is given by complex conjugate eigenvalues on the unit circle in the complex plane. As the saddle nature of the equilibrium point about which the periodic orbit is described will dominate the flow in the region in which the linear terms dominate (and thus the region where the Lindstedt-Poincaré approximations are valid), it follows that all of the orbits described in this paper will be unstable. By backward-integrating in the direction of the stable eigenvector (the eigenvector associated with the eigenvalue of the monodromy matrix which is real and less than one), we may describe the stable invariant manifold on which trajectories wind onto the periodic orbit. In Figure 7 we show the portion of the stable invariant manifold of the reference orbit which passes close to the Earth. The solar sail may be injected onto one of these suitable trajectories, and will then naturally wind onto the periodic orbit.

Finally, we note that the analysis presented here is only a first step towards developing a complete understanding of out-of-plane periodic orbits for solar sails. We have made, in this paper, no attempt to analyse the control and stability of solar sail periodic orbits. However, previous work [11] shows that a linear feedback mechanism is sufficient to control onto equilibrium points by variations in the orientation of the sail through the angle γ. As for stability, we have pointed out above how the orbits described in this paper will be

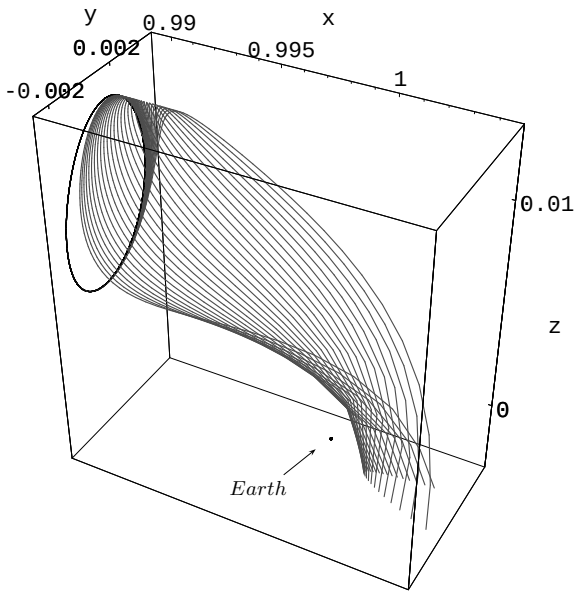

Figure 7. Some possible trajectories for insertion into a large amplitude periodic orbit.

unstable; however by numerically continuing the families of orbits beyond the region where the linear terms dominate we may find regions of stable periodic orbits, as have been found for the classical halo orbits in Breakwell and Brown[6] and Howell,[8] and for solar sails about collinear artificial Lagrange points in McInnes.[3] Some other issues which need to be addressed are the effects of a more realistic non-perfect solar sail, the generalization to an elliptical restricted problem and to include the effects of other bodies such as the Moon.

7. Conclusions

We have analysed the possibility of large amplitude periodic orbits about an out-of-plane equilibrium point in the solar sail circular restricted three body problem. We have found periodic solutions exist naturally at linear order, and we have used these to develop nth order approximations to periodic solutions to the non-linear system using the Lindstedt-Poincaré method. We have shown that we may fine-tune the initial data provided by these approximations to produce closed orbits using a differential corrector. A particular use of such orbits is described: by timing the orbit of the sail appropriately, we can greatly narrow the range in elevation angle of the sail above the local horizon when viewed from the pole. This is a significant improvement compared to a solar sail placed at equilibrium, whose elevation angle has a larger variation over the course of a year.

	x_n	y_n	z_n
$n=2$	$p_{20} = 20.5186\ A_z^2$		$s_{20} = 49.0356\ A_z^2$
	$p_{22} = -3.55591\ A_z^2$	$q_{22} = -12.9483\ A_z^2$	$s_{22} = -14.9348\ A_z^2$
$n=3$		$q_{31} = 2.60431 \times 10^3\ A_z^3$	$s_{31} = 6.24528 \times 10^3\ A_z^3$
	$p_{33} = 47.6633\ A_z^3$	$q_{33} = 345.936\ A_z^3$	$s_{33} = 388.85\ A_z^3$
$n=4$	$p_{40} = 1.15929 \times 10^5\ A_z^4$		$s_{40} = 5.66390 \times 10^5\ A_z^4$
	$p_{42} = -5.01574 \times 10^4\ A_z^4$	$q_{42} = -1.16656 \times 10^5\ A_z^4$	$s_{42} = -1.25391 \times 10^5\ A_z^4$
	$p_{44} = 25.8505\ A_z^4$	$q_{44} = -8612.49\ A_z^4$	$s_{44} = 9809.36\ A_z^4$
$n=5$		$q_{51} = 1.15487 \times 10^8\ A_z^5$	$s_{51} = 2.09916 \times 10^8\ A_z^5$
	$p_{53} = 1.30926 \times 10^6\ A_z^5$	$q_{53} = 5.75586 \times 10^6\ A_z^5$	$s_{53} = 6.1697 \times 10^6\ A_z^5$
	$p_{55} = -3.9207 \times 10^4\ A_z^5$	$q_{55} = 1.95216 \times 10^5\ A_z^5$	$s_{55} = 2.29022 \times 10^5\ A_z^5$
$n=6$	$p_{60} = 5.70222 \times 10^9\ A_z^6$		$s_{60} = 1.99225 \times 10^{10}\ A_z^6$
	$p_{62} = -1.58973 \times 10^9\ A_z^6$	$q_{62} = -4.2924 \times 10^9\ A_z^6$	$s_{62} = -4.72735 \times 10^9\ A_z^6$
	$p_{64} = -2.12349 \times 10^7\ A_z^6$	$q_{64} = -2.0934 \times 10^8\ A_z^6$	$s_{64} = -2.29614 \times 10^8\ A_z^6$
	$p_{66} = 2.12236 \times 10^6\ A_z^6$	$q_{66} = -3.73013 \times 10^6\ A_z^6$	$s_{66} = -4.62427 \times 10^6\ A_z^6$
$n=7$		$q_{71} = 3.72386 \times 10^{12}\ A_z^7$	$s_{71} = -7.02224 \times 10^{12}\ A_z^7$
	$p_{73} = 4.17754 \times 10^{10}\ A_z^7$	$q_{73} = 2.12219 \times 10^{11}\ A_z^7$	$s_{73} = 2.29903 \times 10^{11}\ A_z^7$
	$p_{75} = -3.39622 \times 10^8\ A_z^7$	$q_{75} = 6.45636 \times 10^9\ A_z^7$	$s_{75} = 7.29761 \times 10^9\ A_z^7$
	$p_{77} = -8.33284 \times 10^7\ A_z^7$	$q_{77} = 4.53183 \times 10^7\ A_z^7$	$s_{77} = 6.60065 \times 10^7\ A_z^7$
	$\omega_2 = -2030.41\ A_z^2, \qquad \omega_4 = -7.20375 \times 10^6\ A_z^4, \qquad \omega_6 = -4.08502 \times 10^{11}\ A_z^6$		

Table 1. The coefficients of the seventh order Lindstedt-Poincaré approximations about the reference equilibrium point, $x_e = 0.9895,\ z_e = 0.0078$**.**

Acknowledgments

This work was funded by grant EP/D003822/1 from the UK Engineering and Physical Sciences Research Council (EPSRC). The authors wish to thank two anonymous reviewers for their helpful comments and suggestions.

References

[1]McInnes, C., McDonald, A., Simmons, J., and McDonald, E., "Solar sail parking in restricted three-body systems," *Journal of Guidance, Control and Dynamics*, Vol. 17, No. 2, 1994, pp. 399–406.

[2]Baoyin, H. and McInnes, C., "Solar sail halo orbits at the Sun-Earth artificial L_1 point," *Celestial Mechanics and*

Dynamical Astronomy, , No. 94, 2006, pp. 155–171.

[3]McInnes, A., "Strategies for solar sail mission design in the circular restricted three-body problem," *Masters Thesis, Purdue University*, 2000.

[4]Farquhar, R., "The Control and Use of Libration-Point Satellites," *Ph.D. Dissertation, Stanford University*, 1968.

[5]Farquhar, R. and Kamel, A., "Quasi-periodic orbits about the trans-lunar libration point," *Celestial Mechanics*, Vol. 7, 1973, pp. 458–473.

[6]Breakwell, J. and Brown, J., "The 'halo' family of 3-dimensional periodic orbits in the Earth-Moon restricted 3-body problem," *Celestial Mechanics*, Vol. 20, 1979, pp. 389–404.

[7]Richardson, D. L., "Halo orbit formulation for the ISEE-3 mission," *J. Guidance and Control*, Vol. 3, No. 6, 1980, pp. 543–548.

[8]Howell, K., "Three-dimensional, periodic, 'halo' orbits," *Celestial Mechanics*, Vol. 32, 1984, pp. 53–71.

[9]Thurman, R. and Worfolk, P., "The geometry of halo orbits in the circular restricted three-body problem," *Technical report GCG95, Geometry Center, University of Minnesota*, 1996.

[10]Baoyin, H. and McInnes, C., "Solar sail orbits at artificial Sun-Earth Lagrange points," *Journal of Guidance, Control and Dynamics*, Vol. 28, No. 6, 2005, pp. 1328–1331.

[11]Baoyin, H. and McInnes, C., "Solar sail equilibria in the elliptical restricted three-body problem," *Journal of Guidance, Control and Dynamics*, Vol. 29, No. 3, 2006, pp. 538–543.

[12]Morrow, E., Scheeres, D., and Lubin, D., "Solar sail orbit operations at asteroids," *Journal of Spacecraft and Rockets*, Vol. 38, No. 2, 2001, pp. 279–286.

[13]McInnes, C. R., "Artificial Lagrange points for a non-perfect solar sail," *Journal of Guidance, Control and Dynamics*, Vol. 22, No. 1, 1999, pp. 185–187.

[14]Forward, R., "Statite: a spacecraft that does not orbit," *Journal of Spacecraft and Rockets*, Vol. 28, No. 5, 1991, pp. 606–611.

[15]Crison, M. and Dittberner, G., "Advanced technologies for future environmental satellite systems," *Paper 1.2, 13th Conference on Satelite Meterology and Oceanography, Norfolk, Virginia*, 2004.

[16]McInnes, C. R., *Solar sailing: technology, dynamics and mission applications*, Springer Praxis, London, 1999.

[17]Betounes, D., *Differential Equations: theory and applications*, Springer-Verlag, New York, 2001.

[18]Grimshaw, R., *Nonlinear ordinary differential equations*, Blackwell Scientific Publications, 1990.